Arabian Journal for Science and Engineering (2023) 48:789–801
https://doi.org/10.1007/s13369-022-06968-2

RESEARCH ARTICLE-PHYSICS

Mie Scattering Theory for Identifying Surface Plasmon Resonances (SPR) by the Finite-Size Model: Theoretical Study of Gold-Silver Core–Shell Nanospheres

Ahmad Nurul Fahri[1] · Heryanto Heryanto[1] · Dahlang Tahir[1]

Received: 20 January 2022 / Accepted: 12 May 2022 / Published online: 28 June 2022

Abstract
The Mie scattering theory investigates the optical, electric, and magnetic properties of the gold nanospheres. It explains the nanospheres plasmonic phenomenon in a vacuum and metallic medium by using the finite-size model. It also investigated the effect of particle radius on these properties by varying the radius from 10 to 50 nm. We reported that the optical efficiency shows the existence of plasmon surrounding the nanoparticle, and the polarizability explains the quantity of the plasmon. In addition, the polarizability increases at the specific incident energy of electromagnetic waves which indicated the existence of the plasmon surrounding the nanosphere particle.

Keywords Plasmon · Mie scattering theory · Optical · Electric · Magnetic · Radius

1 Introduction

The integrated devices plasmonic based in the nanoscale region have attracted attention of the scientists for development research in manipulating light [1–3]. Metallic nanosphere (MNS) is the crucial factor for developing plasmonic-based devices due to the ability in the absorption of visible light to generate localized surface plasmonic resonance (SPR) [4, 5]. The SPR absorption band is highly dependent on the size, shape, and the nanoparticle–matrix interface, which is identified from the intensity and energy position of the optical and dielectric properties [5, 6]. The metallic nanostructures with tunable localized SPR are potential applications for optical imaging [7], material characterization research [8], EM wave absorber material [9], drugs delivery [10], meta-material [11], magnetic recording, data storage [12], surface-enhanced Raman scattering [13], and biosensing [14].

The optical, electric, and magnetic properties of nanoparticle-matrix are the basic and essential knowledge for technology development [15–18]. The optical response of nanoparticle-matrix is necessary for tunable localized SPR phenomena [11, 16, 19–21]. This phenomenon is due to the electron at the surface nanoparticle moving and oscillating together to form a short single dipole moment [6, 22] when the EM wave is incident on the nanoparticles. Some SPR was reported by different matrices using configurations of core–shell nanoparticles: Au with Ag coating (SPR at 525–505 nm) [23], Au–ZnO nanocomposites (SPR at 505–615 nm), and gold nanoparticle embedded with silicon (SPR at 539–583 nm) [24].

The Mie scattering theory was used for identifying phenomena of SPR by determining the optical properties and dielectric function [6, 25]. This theory solves the scattering phenomena in many shapes of nanoparticles [6, 20, 26, 27], nanorings [6, 28], cubes [29], and nano-strip structures [30, 31]. For the experimental report of the solid form, Ref [32] analyzed the SPR of gold nanoparticles coated with pure metallic material, and Ref [9] was reported for nanoparticle Fe_3O_4 and analyzed their scattering phase. Reference [8] reported the absorption efficiency of gold nanofluids based on the Mie scattering theory.

The magnetic polarizability and electric polarizability are fundamental properties that influence the performance of the plasmonic-based device which is needed to understand well the efficient future experimental conditions. For the nanoparticle coated with fluid as a medium, Ref. [33] reported and analyzed the effective electric polarizability using Mie scattering theory with four models: virtual cavity, real cavity,

✉ Dahlang Tahir
dtahir@fmipa.unhas.ac.id

[1] Department of Physics, Hasanuddin University, Makassar 90245, Indonesia

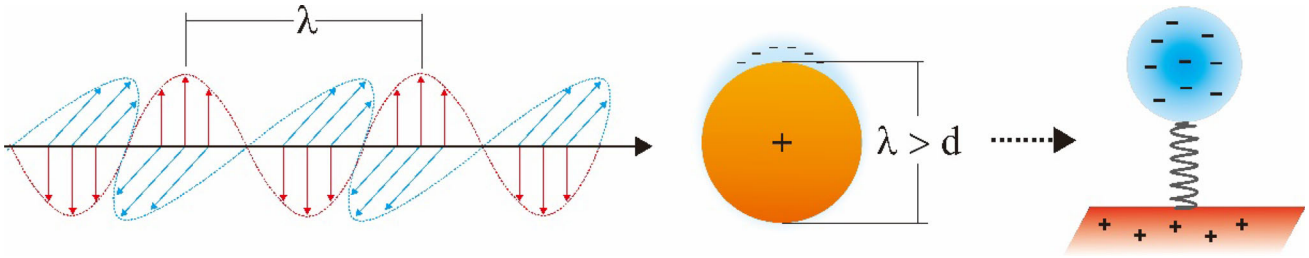

Fig. 1 The SPR in the metallic nanosphere can be modeled like a spring-mass harmonic oscillator derived from Ref. [5]

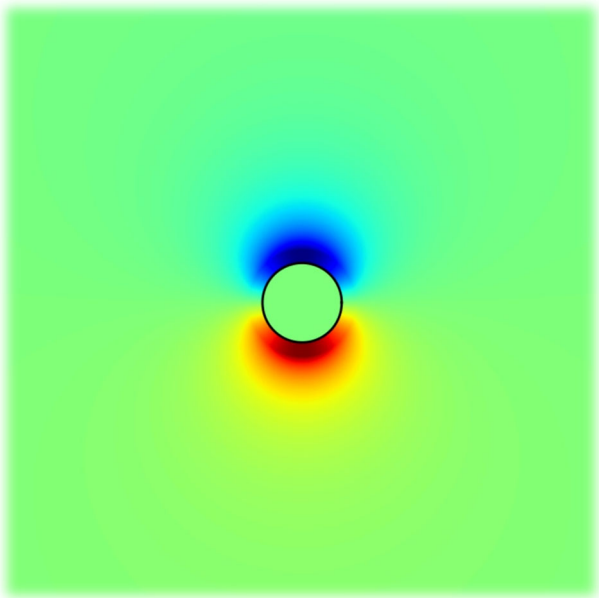

Fig. 2 Schematic illustration of dipole-electric polarizability when the EM incoming to the gold nanosphere the blue color is electron cloud and red to yellow is hole cloud, and green is a medium

hard-sphere, and finite-size model. Their results show that more than 90% agree well between the models with the exact solution for the gas molecule in the medium water. For solid as a medium, there are no references for analyzing electric polarizability of nanosphere using Mie scattering theory which is essential for plasmonic-based devices.

Some models can identify the SPR properties based on their polarizability characteristics, but very few for the finite-size model. Hence, in this study, we applied only the finite-size model [33] to identify EM waves' effect on the localized SPR of hard gold nanosphere for various radii with silver as the medium. This study's model and calculation methods are extinction and scattering efficiency, electric and magnetic polarizability, and absorption properties as a function of nanosphere radius. We found the maximum imaginary part peak position of electric polarizability at 1.17 eV. This peak corresponds to the energy plasmon longitudinal resonance in the conduction band of the gold nanosphere in the silver medium.

2 Model and Calculation Method

For illustration, how to excite SPR when the EM waves are incoming to the metallic nanoparticle by creating dipole charge like a spring-mass of the harmonic oscillator, is shown in Fig. 1 [5]. Figure 2 illustrates dipole electric polarizability at the nanoparticle's surface when the EM wave is incoming. The electron cloud on one side of the surface metallic nanosphere and the hole cloud on another side for a radius smaller than the propagation wavelength show different SPR colors (Fig. 2). The SPR, as a response to the electric field analysis using Mie scattering theory, can be expressed by the dipole electric polarizability [5]. Several references reported the models used to identify and describe the SPR properties of nanoparticles based on their polarizability characteristics, as shown in Table 1.

2.1 Extinction and Scattering Efficiency

The main concept to understand the resonance when the EM waves hit the nanosphere is by observing the optical properties in the form of scattering and extinction part. The efficiencies energy of these properties is defined from the main peak [27]:

$$Q_{sca} = \frac{2}{x^2}\sum_{l=1}^{\infty}(2l+1)\left(\left|t_l^E\right|^2 + \left|t_l^M\right|^2\right) \tag{1}$$

$$Q_{ext} = \frac{2}{x^2}\sum_{l=1}^{\infty}(2l+1)\Re\left\{t_l^E + t_l^M\right\} \tag{2}$$

with $x = \frac{2\pi R}{\lambda}$ [27], l is the orbital momentum number, and t_l^E and t_l^M are the Lorenz–Mie coefficients [6, 25]:

$$t_l^E = \frac{-\varepsilon_m j_l(\rho_m)\left[j_l(\rho)+\rho j_l'(\rho)\right] + \varepsilon j_l(\rho)\left[j_l(\rho_m)+\rho_m j_l'(\rho_m)\right]}{\varepsilon_m h_l^{(+)}(\rho_m)\left[j_l(\rho)+\rho j_l'(\rho)\right] - \varepsilon j_l(\rho)\left[h_l^{(+)}(\rho_m)+\rho_m h_l^{(+)'}(\rho_m)\right]} \tag{3}$$

Table 1 Mie theory-based model describing the SPR characteristics from the phenomena particle's polarizability of various theoretical studies. We also provided the physical phenomena and conclusion which are strongly dependent on the method or model and type of particle

Material	Model/method	Equation	Physical Phenomena	Conclusion	References
Gas molecules (CH_4, CO_2, N_2O, O_3, etc.) in the medium of water	Local field corrected	$\alpha^* = \left(\frac{\varepsilon+2}{3}\right)^2 \alpha$	Known also as the virtual cavity model, which describes the change of the electric field caused by a dielectric sphere. It is describing the connection between the quantity of microscopic polarizability and dielectric function	For the case of gases molecule, the best approximation that can be used is the finite-size model which has > 99% agreement with the exact value. This model strongly depends on the R and R_C because of the multiple reflections, which also indicate that this model might fail for a larger object like fullerene	[33]
	Onsager	$\alpha^* = \left(\frac{3\varepsilon}{1+2\varepsilon}\right)^2 \alpha$	It is considering a vacuum layer located between the particle and the medium. For typical cavity radii, it has > 99% agreement compared with the exact solution		
	Hard sphere	$\alpha^* = 4\pi\varepsilon_0 R_s \frac{3\varepsilon_s - \varepsilon}{\varepsilon_s + 2\varepsilon}$	This model describes that the hard-sphere particle's polarizability arises when the vacuum layer vanishes		
	Finite-size	$\alpha_C^* = 4\pi\varepsilon_0\varepsilon R_C \frac{1-\varepsilon}{1+2\varepsilon}$ $\alpha_s = 4\pi\varepsilon_0 R^3 \frac{\varepsilon_s - 1}{\varepsilon_s + 2}$ $\alpha^* = \alpha_C^* + \alpha_s \left(\frac{3\varepsilon}{2\varepsilon+1}\right)^2 \frac{1}{1+\alpha_C^*\alpha_s/(8\pi^2\varepsilon_0^2 R_C^6 \varepsilon)}$	Describe the excess polarizability of a three-layered system (free-space donated as α_s, cavity donated as α_C^*, and the particle which is taken from the hard-sphere model). The performed results have > 99% agreement with the exact value for small molecules		
Gold and silver, which are in the form of an ellipsoid, disk, and ring	Lorentz-Mie using Boundary Element Method	$t_l^E = \frac{-\varepsilon_m j_l(\rho_m)\left[j_l(\rho)+\rho j_l'(\rho)\right]+\varepsilon j_l(\rho)\left[j_l(\rho_m)+\rho_m j_l'(\rho_m)\right]}{\varepsilon_m h_l^{(+)}(\rho_m)\left[j_l(\rho)+\rho j_l'(\rho)\right]-\varepsilon j_l(\rho)\left[h_l^{(+)}(\rho_m)+\rho_m h_l^{(+)'}(\rho_m)\right]}$ $t_l^M = \frac{-\rho j_l(\rho_m) j_l'(\rho)+\rho_m j_l'(\rho_m) j_l(\rho)}{\rho h_l^{(+)}(\rho_m) j_l'(\rho)-\rho_m h_l^{(+)'}(\rho_m) j_l(\rho)}$ $\alpha_E = \frac{3t_l^E}{2k^3}$ $\alpha_M = \frac{3t_l^M}{2k^3}$	This research describes the role of magnetic absorption produced by anisotropy in non-spherical particles. It describes that the role of magnetic absorption is strongly modified by the anisotropy and is higher when the electric field is oriented along the narrower direction of the particle. This phenomenon can be understood from the dissipation of eddy currents produced by the variation of the magnetic field which takes place at frequencies above the plasmonic resonances	The magnetic absorption of a particle is affected by its anisotropy and the electric field incidence direction	[6]

Table 1 (continued)

Material	Model/method	Equation	Physical Phenomena	Conclusion	References
Nano-sized and micron-sized Fe_3O_4	Lorentz-Mie Method using MATLAB and COMSOL for the scattering calculation	$a_l = \frac{j_l'(y)j_l(x) - mj_l(y)j_l'(x)}{j_l'(y)h_l^{(+)}(x) - mj_l(y)h_l^{(+)'}(x)}$ $b_l = \frac{mj_l'(y)j_l(x) - j_l(y)j_l'(x)}{mj_l'(y)h_l^{(+)}(x) - j_l(y)h_l^{(+)'}(x)}$ $c_l = \frac{m\left[j_l'(x)h_l^{(+)}(x) - j_l(y)h_l^{(+)'}(y)\right]}{j_l'(y)h_l^{(+)}(x) - mj_l(y)h_l^{(+)'}(x)}$ $d_l = \frac{m\left[j_l'(y)h_l^{(+)}(x) - j_l(y)h_l^{(+)'}(y)\right]}{mj_l'(y)h_l^{(+)}(x) - j_l(y)h_l^{(+)'}(x)}$	Based on MATLAB calculation using Mie theory as the basis, the scattering and absorption properties of nanoscale and micro-scale Fe3O4 are not the same, where the micro-scale particle is better than the nanoscale one. The modeling analysis using COMSOL, when an EM wave (2–18 GHz) passes through a spherical space where nanosized Fe3O4 particles are randomly distributed, the analysis shows that as the increase of frequency, the dielectric loss increases first and then decrease. Besides that, the magnetic loss increases with the increase of EM frequency	According to the particle's scale, the micro-scale particles of Fe_3O_4 have better scattering and absorption properties compared to the nanoscale one. The energy loss property of a single nanoscale of Fe3O4 obtained by Mie theory (MATLAB) and COMSOL was also compared, and it is concluded that the trend and the values of Mie theory are different from that COMSOL calculation	[9]
Artificial nanoparticle	Lorentz-Mie method using Weierstrass factorization	$\varphi_l^{(\pm)}(x) \equiv \frac{\left[xh_l^{(\pm)}(x)\right]'}{h_l^{(\pm)}(x)}$ $\varphi_l^{(1)}(x) \equiv \frac{[xj_l(x)]'}{j_l(x)}$ $a_l = \frac{j_l(\rho_m)}{h_l^{(+)}(\rho_m)} \frac{\varepsilon\varphi_l^{(1)}(\rho_m) - \varepsilon_m\varphi_l^{(1)}(\rho)}{\varepsilon\varphi_l^{(+)}(\rho_m) - \varepsilon_m\varphi_l^{(1)}(\rho)}$ $a_{QS} = \frac{-2iz^3}{3} \frac{\varepsilon - \varepsilon_m}{\varepsilon + 2\varepsilon_m}$ $\varepsilon \to \varepsilon_{eq}$ $\varepsilon_{eq} = \left(\frac{a}{\rho_0}\right)^2 \frac{1 - (\rho_0/a)^2\varepsilon}{1 - (\rho_0/b)^2\varepsilon}$	The point-like model (a_{QS}) fail to predict the strong electric dipolar resonance of the dielectric particle. The replacement of $\varepsilon \to \varepsilon_{eq}$ could solve this problem which that shows the strong resonance and matched accurately to the exact Mie calculation. This provides a way to describe the EM dipolar resonance of metallic and dielectric particles	The dielectric particles can represent the same EM dipolar response as metallic particles. This analytical approach shows that localized surface plasmon resonance can only be achieved by dielectric material with high permittivity values	[22]

Table 1 (continued)

Material	Model/method	Equation	Physical Phenomena	Conclusion	References
Artificial nanoparticle	Lorentz-Mie method	$a_l = \frac{m^2 j_l(m\rho)[\rho j_l(\rho)]' - \mu j_l(\rho)[m\rho j_l(m\rho)]'}{m^2 j_l(m\rho)\left[\rho h_l^{(+)}(\rho)\right]' - \mu h_l^{(+)}(\rho)[m\rho j_l(m\rho)]'}$ $b_l = \frac{\mu j_l(m\rho)[\rho j_l(\rho)]' - j_l(\rho)[m\rho j_l(m\rho)]'}{\mu j_l(m\rho)\left[\rho h_l^{(+)'}(\rho)\right] - h_l^{(+)}(\rho)[m\rho j_l(m\rho)]'}$ $j_1(x) \approx \frac{x}{3\left(1+\frac{1}{10}x^2\right)} \quad j_2(x) \approx \frac{x^2}{15\left(1+\frac{1}{14}x^2\right)}$ $h_1^{(+)}(x) \approx \frac{-i-\frac{2}{3}x-i\frac{1}{2}x^2}{x^2-i\frac{2}{3}x^3} \quad h_2^{(+)}(x) \approx \frac{-3i-i\frac{x^2}{2}}{x^3}$ $[xj_1(x)]' \approx \frac{2x}{3\left(1+\frac{1}{5}x^2\right)} \quad [xj_2(x)]' \approx \frac{x^2}{5\left(1+\frac{5}{42}x^2\right)}$ $\left[xh_1^{(+)}(x)\right]' \approx \frac{i+\frac{4}{3}x-i\frac{x^2}{2}x^2}{x^2-i\frac{4}{3}x^3} \quad \left[xh_2^{(+)}(x)\right]' \approx i\frac{6}{x^3}$ $Q_{\text{sca}} = \frac{2}{x^2}\sum_{l=1}^{\infty}(2l+1)\left(\lvert a_l\rvert^2 + \lvert b_l\rvert^2\right)$ $Q_{\text{ext}} = \frac{2}{x^2}\sum_{l=1}^{\infty}(2l+1)R\{a_l + b_l\}$	The enhancement of the electric Mie coefficient, a_l, corresponding to the plasmonic region resonance characteristic of a sphere. Along with the scattering efficiency of the sphere, that the magnetic coefficient shows a clear distribution of circulating charge, resembling the manner of magnetic dipoles, quadrupoles, and octupoles in such a way. The electric coefficient also shows that the surface charge accumulates in a dipolar, quadrupolar, and octupolar manner which that the plasmonic and dielectric electric resonances exhibit the same surface strength and charge distribution	Mie coefficient can describe the energy balance for different mechanisms on a sphere which is expressed by looking into its far-field characteristics, i.e., the scattering and extinction efficiencies. These characteristics then can be used to observe the lines of radiation enhancement in both the plasmonic ($\varepsilon < 0$) and dielectric ($\varepsilon > 0$) region	[26]
Gold nanoparticle	Clausius–Mossotti relation with radiation reaction correction	$\alpha_{\text{CM}} = 3\varepsilon_0 V \frac{\varepsilon-\varepsilon_m}{\varepsilon+2\varepsilon_m}$ $V \to V_{\text{eff}}$ $V_{\text{eff}} = 4\pi\int_0^R r^2 e^{\frac{r-R}{\delta}}\,\mathrm{d}r$ $\delta = \frac{\lambda}{2\pi\,\text{Im}\{\varepsilon^{1/2}\}}$ $a_{\text{RR}} = \alpha_{\text{CM}}\left[1 - \frac{ik^3}{6\pi\varepsilon_0}\alpha_{\text{CM}}\right]^{-1}$	The model which used in this study was radiation reaction correction which corrects the back-action of the scattered field on the dipole moment which only become significant at $\frac{\lambda}{50} < r < \lambda/2$. This model is quite significant in calculating the scattering forces but less significant for calculating gradient forces. Without using this model, the error of scattering forces is > 20%. This result component shows an agreement with MST and FDTD simulation results	The use of the effective volume (V_{eff}) approach in calculating polarizability is not accurate because a complex-valued ε already fully explains the field attenuation in the particle skin. But this issue can be overcome by adding the radiation reaction correction to the CM relation for scattered far field and optical force	[34]

Table 1 (continued)

Material	Model/method	Equation	Physical Phenomena	Conclusion	References
Gold nanoparticle	Lorentz-Mie and some numerical methods (BEM, DDA, FDTD)	$t_l^E = \frac{-\varepsilon_m j_l(\rho_m)\left[j_l(\rho)+\rho j_l'(\rho)\right]+\varepsilon j_l(\rho)\left[j_l(\rho_m)+\rho_m j_l'(\rho_m)\right]}{\varepsilon_m h_l^{(+)}(\rho_m)\left[j_l(\rho)+\rho j_l'(\rho)\right]-\varepsilon j_l(\rho)\left[h_l^{(+)}(\rho_m)+\rho_m h_l^{(+)'}(\rho_m)\right]}$ $\alpha_E \begin{cases} \left(\frac{3\lambda^3}{4\pi^2}\right) t_{l=1}^E, \; d \sim 150 \text{ nm} \\ 3V\varepsilon_m \frac{1-\frac{0.1(\varepsilon+\varepsilon_m)\rho^2}{4}}{\frac{\varepsilon+2\varepsilon_m}{\varepsilon-\varepsilon_m}-\frac{(0.1\varepsilon+\varepsilon_m)\rho^2}{4}-i\left(\frac{2}{3}\right)\varepsilon_m^{\frac{3}{2}}\rho^3}, \text{ small radii} \end{cases}$ $j_1(x) = \frac{\sin x}{x^2} - \frac{\cos x}{x} \quad h_1^{(+)}(x) = \left(\frac{1}{x^2} - \frac{i}{x}\right)\exp(ix)$	The Mie theory shows a red-shift with increasing the particle size and the higher-order multipoles arise in large particles. The particle responds as an induced dipole for diameter < 150 nm where the higher-multipole modes become stronger at a larger size of the particle. The multipoles also arise in the interaction between the neighboring particles even for small diameters. Plasmonic characteristics for the other shapes of particle-like rods and ellipsoid were then obtained using BEM which a redshift was also observed with increasing aspect ratio and particle length in both shapes. The numerical method such as BEM, DDA, and FDTD was then used to solve the complexity of the EM field in the presence of arbitrary-shaped nanoparticle. Some advantages and disadvantages of those numerical methods are also discussed such as the computational and storage demand, the complexity of parameterization, time-consuming, etc	Some numerical methods are quite significant for predictive simulations of optical spectra where the methods yield the solution to Maxwell's equations. A description of the plasmonic property in metallic nanoparticles for spheres, ellipsoids, and nanorods is generally possible using analytical formulae. More accurate results for arbitrary shapes of particles must rely on the numerical method	[25]
Left-Handed Metamaterial	Lorentz-Mie method with Lewin's Model	$a_l = \frac{mj_l(m\rho)j_l'(\rho)-j_l(\rho)j_l'(m\rho)}{mj_l(m\rho)h_l^{(+)'}(\rho)-j_l'(m\rho)h_l^{(+)}(\rho)}$ $b_l = \frac{j_l(m\rho)j_l'(\rho)-mj_l(\rho)j_l'(m\rho)}{j_l(m\rho)h_l^{(+)'}(\rho)-mj_l'(m\rho)h_l^{(+)}(\rho)}$ $\varepsilon_{\text{eff}} = \varepsilon_m\left(1+\frac{3v_f}{\frac{F(\theta)+2b_e}{F(\theta)-b_e}-v_f}\right)$ $\mu_{\text{eff}} = \mu_m\left(1+\frac{3v_f}{\frac{F(\theta)+2b_m}{F(\theta)-b_m}-v_f}\right)$ $F(\theta) = \frac{2(\sin\theta-\theta\cos\theta)}{(\theta^2-1)\sin\theta+\theta\cos\theta}$ $b_e = \varepsilon_m/\varepsilon \quad b_m = \mu_m/\mu$	Electric and magnetic responses as resonance effects is a necessary condition for fabricating the LHMs which these responses strongly depend on the dielectric properties and geometrical dimension of the object. Negative values of the response were only achieved over a narrow frequency range near the resonances, especially for the magnetic	The rapid development of Left-Handed Metamaterials (LHMs) makes Lewin's model introduced into the realm of metamaterials to actualize single and double negative media. In this model, the notable parameters are formulated only considering the resonant fields in either the first or second resonant mode of the Mie series	[35]

$$t_l^M = \frac{-\rho j_l(\rho_m) j_l'(\rho) + \rho_m j_l'(\rho_m) j_l(\rho)}{\rho h_l^{(+)}(\rho_m) j_l'(\rho) - \rho_m h_l^{(+)'}(\rho_m) j_l(\rho)} \tag{4}$$

$\rho = (kR)\sqrt{\varepsilon}$, $\rho_m = (kR)\sqrt{\varepsilon_m}$, $j_l(x)$ and $h_l^{(+)}(x)$ are Bessel and Hankel function, respectively, R is particle radius, ε and ε_m are particle and medium permittivity, respectively, and quotation mark ($'$) indicated the derivative of the function. For dipole case ($l = 1$), the Bessel and Henkel function becomes $j_1(a) = \frac{\sin a}{a^2} - \frac{\cos a}{a}$ and $h_1^{(+)}(a) = \left(\frac{1}{a^2} - \frac{i}{a}\right)\exp(ia)$, respectively [25]. Dielectric function of material can be approximate by using classical EM solution in the form of Drude dielectric function [6, 25]:

$$\varepsilon(\omega) \approx 1 - \frac{\omega_p^2}{\omega(\omega + i\gamma)} \tag{5}$$

where ω_p and γ is the phonon frequency and attenuation coefficient, respectively. ω_p and γ for gold as input parameters were taken from ref. [6].

2.2 Electric and Magnetic Polarizability

Mie scattering theory is used to explain EM waves' scattering by a nanospherical object [10]. The electric and magnetic polarizability of a nanospherical material in a vacuum is described as follows [6, 25]:

$$\alpha_E = \frac{3t_l^E}{2k^3} \tag{6}$$

$$\alpha_M = \frac{3t_l^M}{2k^3} \tag{7}$$

where $k = 2\pi/\lambda$ and λ is the wavelength.

2.3 Electric Polarizability Models

The electric polarizability models for particles embedded in a medium are approximate. In this study, we use a finite-size model for determining the electric polarizability of a particle in a solid medium. This model combines electric polarizability in a vacuum and a hard sphere [12, 33]. The hard-sphere model describes the electric polarizability of the nano-hard-sphere object in a medium with input parameters such as hard sphere radius and permittivity, and medium permittivity, as denoted by R, ε, and ε_{m}, respectively. The relation between these parameters with Mie scattering coefficient α_{HS} is as follows [33]:

$$\alpha_{\mathrm{HS}} = 4\pi\varepsilon_0\varepsilon_m R^3 \frac{\varepsilon - \varepsilon_m}{\varepsilon + 2\varepsilon_m} \tag{8}$$

By using the model above, a model can be explained that has a three-layer system [33]. First is the polarizability of material in a vacuum, which in this study uses the electric polarizability from Mie scattering theory. The excess for the cavity is:

$$\alpha_C = 4\pi\varepsilon_0\varepsilon_m R_C^3 \frac{1 - \varepsilon_m}{1 + 2\varepsilon_m} \tag{9}$$

by substituting Eq. (6) and (9) in Eq. (8):

$$\alpha_{fs} = \alpha_C + \alpha\left(\frac{3\varepsilon_m}{2\varepsilon_m + 1}\right)^2 \frac{1}{1 + \left(\frac{\alpha_C \alpha}{8\pi^2\varepsilon_0^2 R_C^6 \varepsilon_m}\right)} \tag{10}$$

where it is called a finite-size model. The illustration of the model can be seen in Fig. 3, and the computational flowchart in this study is summarized in Fig. 4.

Figure 3 clearly shows the spherical vacuum cavity area between hard sphere gold nanoparticle (radius R) and the solid medium (radius R_{C}). The input parameters for calculation are particle radius of solid gold nanoparticle R, radius of the spherical vacuum cavity R_{C}, phonon frequency ω_{p}, attenuation coefficient γ, and wavelength λ. By using Eqs. 1, 2, 6, and 7, the extinction efficiency, scattering efficiency, electric polarizability and magnetic polarizability were determined, respectively. For more clear details, the computational flowchart for calculation method in this study can be seen in Fig. 4.

2.4 Calculation Method

3 Results and Discussion of Computational Test

3.1 Scattering and Extinction efficiencies

As shown in Fig. 5, both optical efficiencies are in a positive region which indicates that the particle's resonance corresponds to the dielectric resonance. The dielectric characteristic of a particle is described by the electric and magnetic properties (electric polarizability, magnetic absorption, plasmonic characteristics) [26]. The efficiency increases drastically for a small radius (less than the maximum peaks) as the nanosphere radius increases to the point where it reaches a maximum and then decays slowly. For the particle radius 8.7 nm and 13.7 nm, the metallic nanosphere will gain maximum scattering and extinction efficiencies, indicating the highest probability of electron clouds.

3.2 Real and Imaginary Part of Electric Polarizability

Mie scattering theory shows that the electric polarizability of gold nanosphere in vacuum for dipole case increases and moves to the lower energy with the increasing the nanosphere

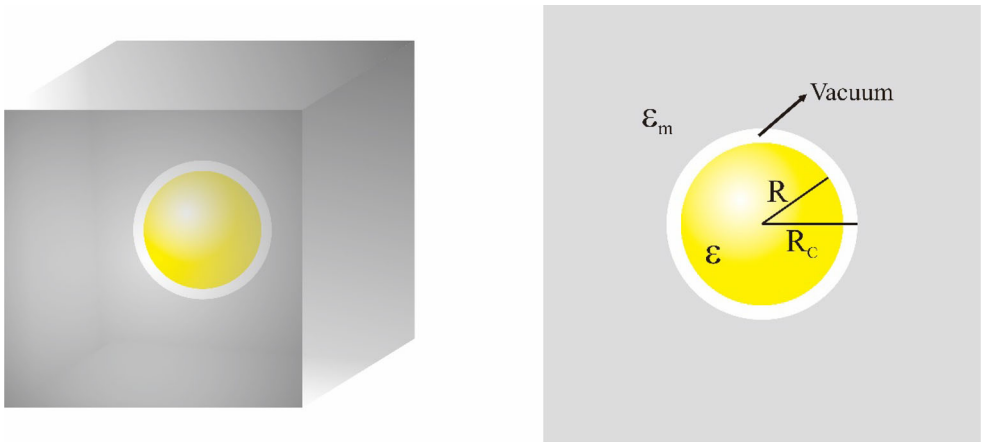

Fig. 3 Finite-size model illustration of particle inside a solid medium for three-dimensional (left) and two-dimensional (right). ε and ε_m are the particle and medium permittivity, respectively, R is the radius of the particle, and R_c is the radius of the spherical vacuum cavity, modification from [33] for molecule in water as a medium

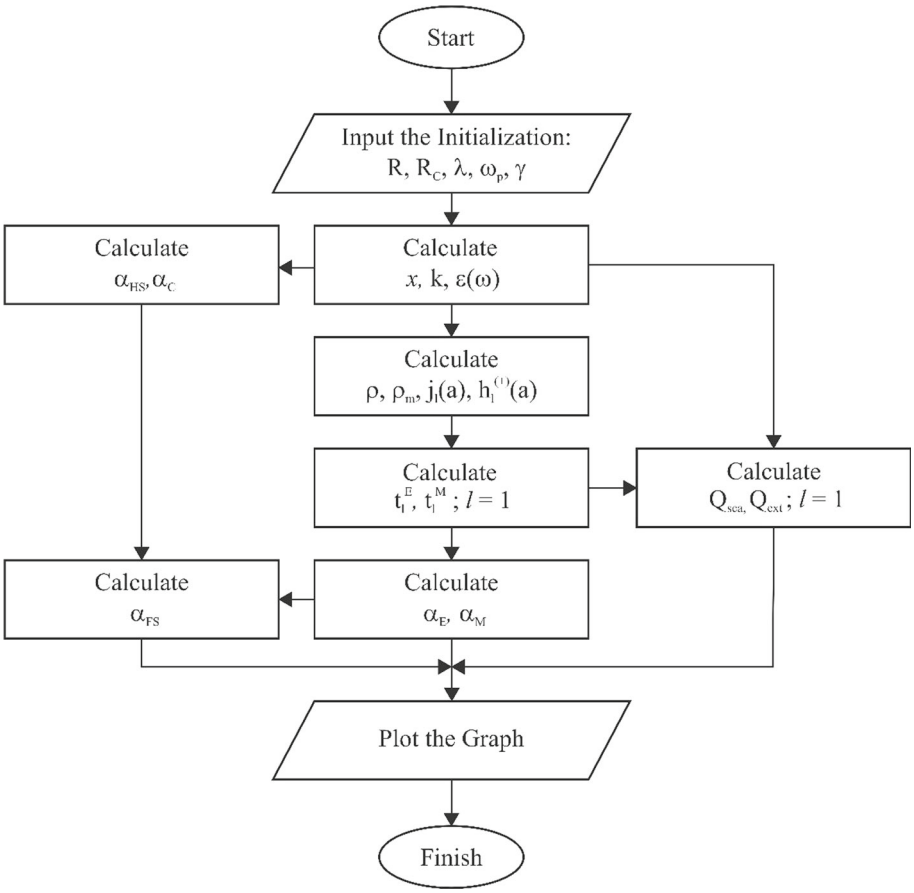

Fig. 4 Computational flowchart using finite-size model based on the Eqs. (1–10) for determining extinction and scattering efficiency (Q_{sca} and Q_{ext}) and electric and magnetic polarizability (α_E and α_M), and electric polarizability from Mie scattering theory (α_{fs}) for particle inside a solid medium where R is the radius of the particle, and R_c is the radius of the spherical vacuum cavity

radius. Figure 6c, d shows the electric polarizability spectra of the gold nanosphere with main peaks value presented in Table 2. The particle radius varied from 10 to 50 nm with an interval value of 10 nm. The real and imaginary part peak data shifted to 0.09 ± 0.02 eV and 0.06 ± 0.01 eV, respectively, to the lower energy with increasing radius of the gold nanosphere. The resonance of the plasmon longitudinal is in the negative value of the real part electric polarizability (−Re{α**E**}) [25]. It indicates that the plasmon longitudinal resonance frequency of the gold nanosphere reaches a maximum for the radius ~ 30– ~ 40 nm as shown in Fig. 6c.

Figure 7 shows the ratio between an imaginary part of magnetic and electric polarizability (Im{α**M**}/Im{α**E**}) of the various radii of gold nanosphere in a vacuum. The insert

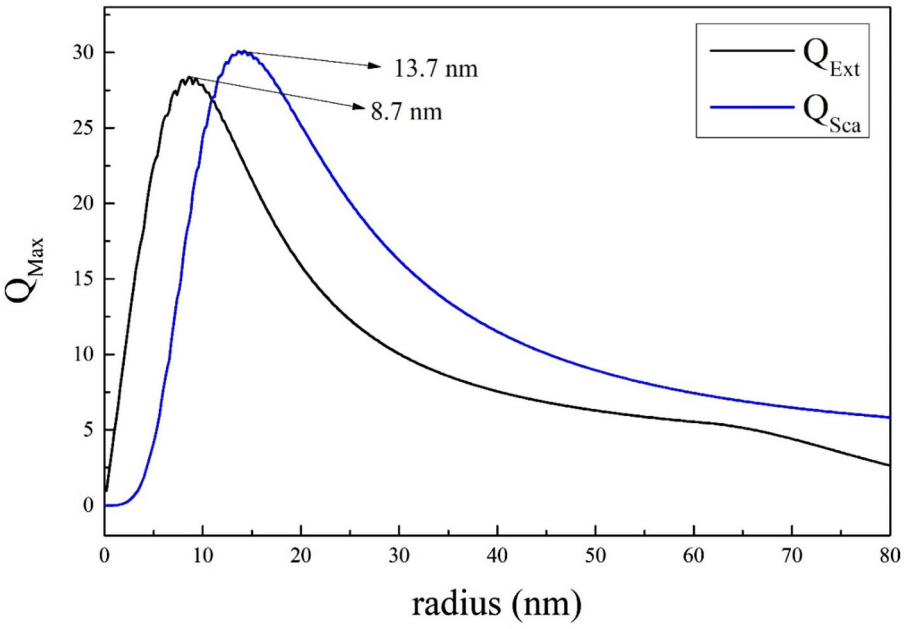

Fig. 5 Scattering and extinction efficiencies of gold nanosphere in vacuum for dipole case ($l = 1$), where l is the orbital momentum number

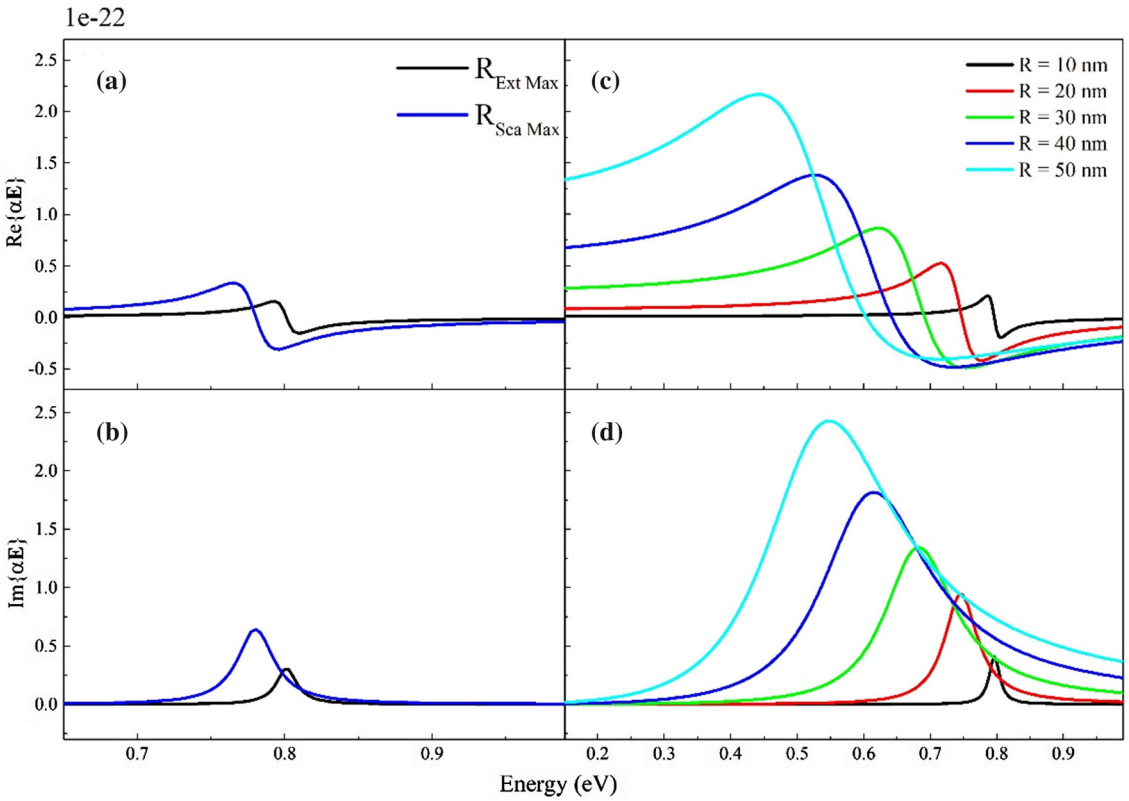

Fig. 6 The real (Re(α**E**)) part (**a, c**) and imaginary (Im(α**E**)) part (**b, d**) of electric polarizability for gold nanosphere in vacuum. **a, b** The radius maximum value of extinction (R_{Ext}) and scattering (R_{Sca}) efficiencies, **c, d** for various radius values of gold nanosphere

Table 2 The main peak for the real (Re(α**E**)) part and imaginary (Im(α**E**)) part of electric polarizability and the ratio between magnetic and electric polarizability of gold nanosphere as a function of energy

R (nm)	Energy (eV)		
	Re{α**E**}	Im{α**E**}	Im{α**M**}/Im{α**E**}
10	0.78	0.79	0.79
20	0.71	0.74	0.74
30	0.62	0.68	0.68
40	0.53	0.61	0.61
50	0.44	0.54	0.54

figure is for skin depth effect ($\delta = \lambda/\left(2\pi \mathrm{Im}\left\{\varepsilon^{\frac{1}{2}}\right\}\right)$) to the magnetic properties [34]. In this study, the volume of the gold nanosphere is fully affected by the incident EM for the radius < ~ 22.5 nm. The magnetic absorption by a metallic nanosphere will produce an Eddy current leading to high imaginary electric polarizability (Im{α**E**}). Consequently, those properties (magnetic absorption and imaginary electric polarizability) have an opposite trend in the same energy position [6].

As shown in the previous explanation, the metallic nanosphere will gain maximum extinction and scattering efficiencies for the sphere's specific radius, as shown in Fig. 7. Equations (1)–(4) show that the efficiencies depend on the size of the nanosphere (x). On the other hand, the electric and magnetic polarizability shows good linear depending on the radius, as shown in Figs. 6 and 7. In contrast, the polarizability depends on Henkel and Bessel function to describe the radius effect. At the same time, the polarizability is affected by the quantity of the plasmon surrounding the particle. It is linearly dependent on the nanosphere radius. The efficiency of the existing plasmon surrounds the particle at a specific radius indicated by the scattering and extinction efficiencies.

Figure 8 shows real and imaginary parts of electric polarizability of the gold nanosphere in a vacuum and silver medium. It indicated specific energy of incident EM waves to the nanosphere to gain the highest electric polarizability. It shows a slight shift of the peak to the higher energy with an increasing radius of gold nanosphere for the particle embedded in a metallic medium which affected the electric polarizability. This model also shows that the electric polarizability increases sharply when the nanosphere is embedded in a metallic medium. This phenomenon indicates the existence of plasmon in the vacuum layer between the nanosphere and the medium. It may occur due to the metallic medium also producing an electron cloud when the EM waves are applied.

Figure 9 shows that the electric polarizability value reaches 1e−20 and 1e−19 for real and imaginary parts, respectively. The maximum position electric polarizability at the imaginary part is 1.17 eV which corresponds to the SPR energy. This energy position is lower than some reported references probably due to the different condition (vacuum) and matrices (solid silver). The Au with Ag coating shows SPR at 525 nm (2.36 eV) to 505 nm (2.46 eV) [23], Au–ZnO nanocomposites at 505 (2.46 eV) nm to 615 nm (2.02 eV), and gold nanoparticle embedded with silicon at 539 nm (2.30 eV)

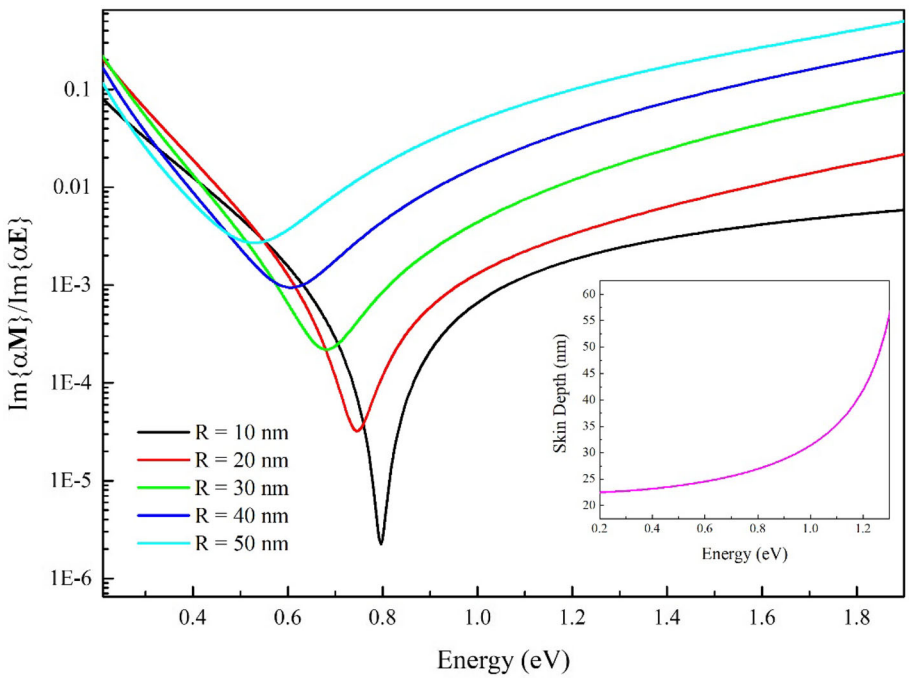

Fig. 7 The ratio between imaginary magnetic and electric polarizability of gold in vacuum for the various gold nanosphere radius. Skin depth shows decrease in magnetic absorption with decreasing the nanosphere radius

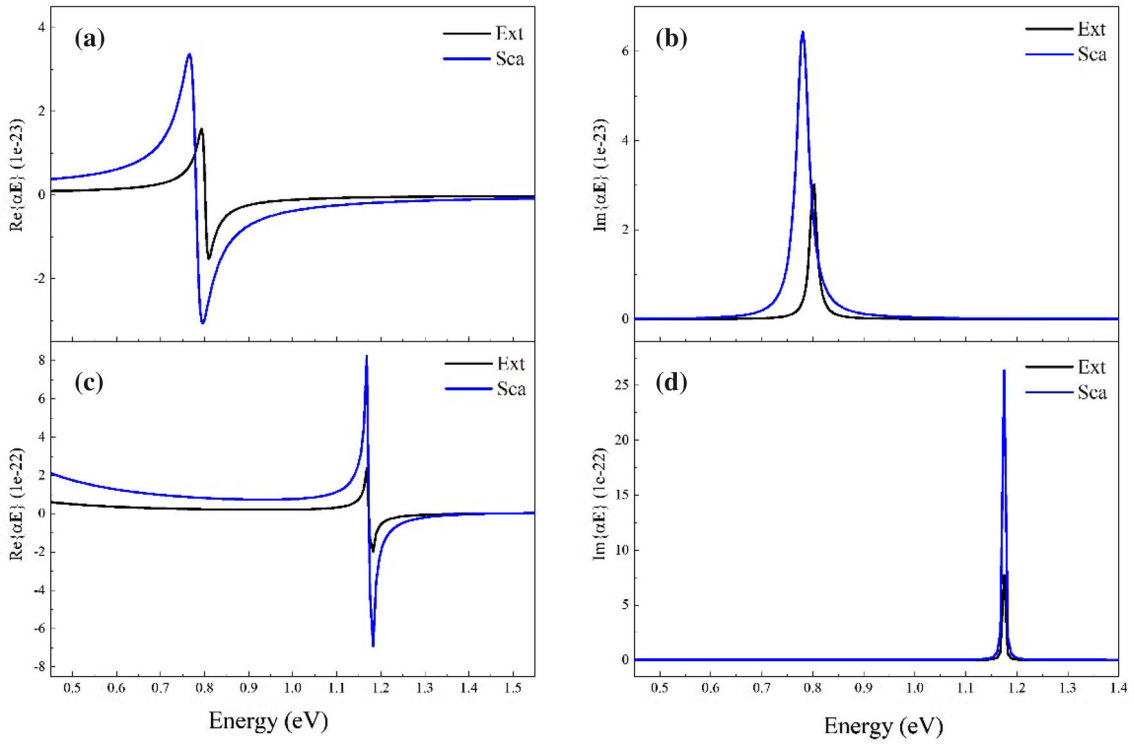

Fig. 8 The complex (Re (αE) and Im (αE)) electric polarizability of gold in vacuum (**a, b**), and in silver medium (**c, d**) for the radius ~ 30–~ 40 nm (at the maximum value of extinction (Ext) and scattering efficiencies (Sca))

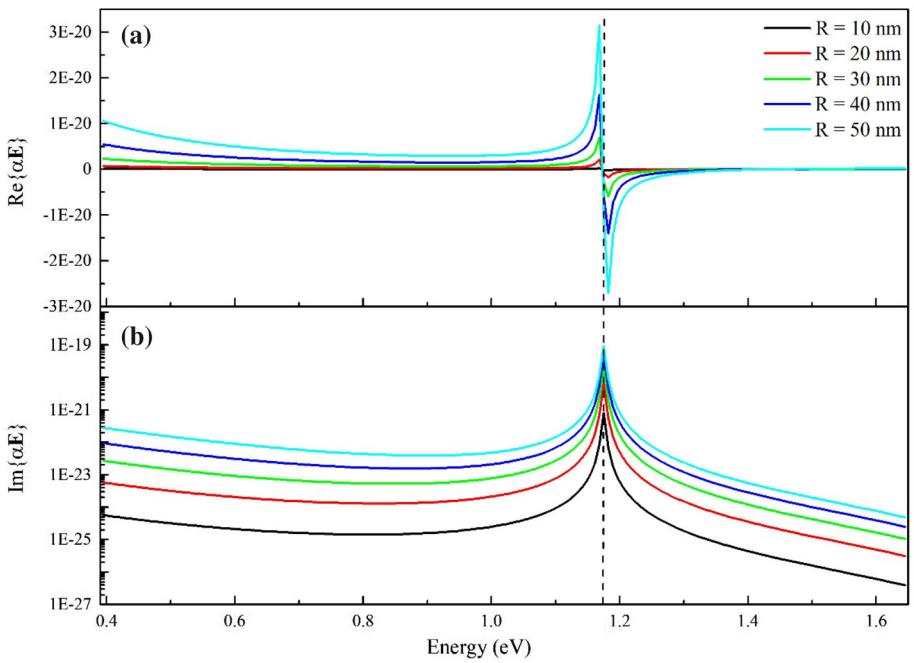

Fig. 9 Electric polarizability of gold nanosphere for the various radius in the silver medium for **a** real part at linear scale and **b** imaginary part at logarithmic scale by using the finite-size model

to 583 nm (2.13 eV) [24]. Figure 9a clearly shows that the real part decreases sharply from the maximum to the negative value due to the imaginary part of electric polarizability in a finite-size model. This phenomenon corresponds to the maximum value of the plasmon longitudinal resonance in the conduction band of the gold nanosphere. Besides that, Fig. 9 shows that electric polarizability gains less negative value for $R \sim R_c$, and more negative value for $R > R_c$ [33].

4 Conclusion, Limitation, and Future Prospects

The extinction and scattering efficiency (Q_{sca} and Q_{ext}), electric and magnetic polarizability (αE and αM), and electric polarizability from Mie scattering theory (αfs) were successfully studied. The electric polarizability is used to analyze the plasmonic phenomena of a metallic nanosphere (gold) in a vacuum and embedded in a metallic medium (silver) using the finite-size model. The main peak of real and imaginary parts of electric polarizability shows shifted 0.09 ± 0.02 eV and 0.06 ± 0.01 eV, respectively, to the lower energy with an increasing radius of gold nanosphere for every 10 nm. The plasmon longitudinal resonance frequency of the gold nanosphere reaches its maximum at a radius of ~ 34 nm. The electric polarizability value reaches 1e−20 and 1e−19 for real and imaginary parts, respectively. The maximum peak position of electric polarizability at the imaginary part is 1.17 eV, indicating the maximum value of the plasmon longitudinal resonance. The resonance takes place in the conduction band of the gold nanosphere, also affected by the ratio of R and R_c.

In this study, we perform only characteristics SPR generated from gold nanosphere embedded by solid silver as a medium. However, for the better application of SPR from gold nanospheres including optical imaging and drugs delivery, there are still some bottlenecks that need to be addressed. First, optical imaging and drugs delivery is a multi-complex system, and interference is still a big problem for the real applications. Functionalization of SPR from gold nanosphere is an effective strategy for the generation of highly stable optical imaging and drugs delivery with high accuracy and affinity for many targets. Nevertheless, much research focused SPR for the novel sensors as an optical imaging and drugs delivery rather than applicability to real samples. Second is impurity materials; therefore, the sensitivity of hard gold nanosphere-based SPR colorimetric sensor is of great importance for optical imaging and drugs delivery. Third, optical imaging drug delivery usually needs on-site operation, so generating SPR from gold nanosphere for the complex system is a realistic challenge and needs to be overcome. Finally, reproducible application of SPR generate from gold nanosphere requires further improvement. Overall, despite the realistic challenge, significant progress has been achieved by theoretical system for the SPR based on metal nanoparticles over the past years. Moreover, numerous methods for generating SPR for optical imaging and drugs delivery have been reported, thus demonstrating the great promise for the application of SPR from metals nanosphere in future.

In future, an increased number of collaborations with scientists from various disciplines to overcome through the collective efforts can be expected, and novel methods for generating SPR from metal nanoparticles. We hopefully by the collaboration will get excellent advantages for developing various applications of SPR from metal nanoparticle including optical imaging and drugs delivery with excellent performance.

References

1. Ahmadivand, A.; Karabiyik, M.; Pala, N.: Plasmonic photodetectors. Photodetect. Mater. Dev. Appl. (2016). https://doi.org/10.1016/B978-1-78242-445-1.00006-3
2. Li, L.; Li, T.; Tang, X.M.; Zhu, S.N.: Plasmonic polarization generator in well-routed beaming. Light Sci. Appl. **4**, 1–5 (2015). https://doi.org/10.1038/lsa.2015.103
3. Fan, X.; Hao, Q.; Qiu, T.; Chu, P.K.: Improving the performance of light-emitting diodes via plasmonic-based strategies. J. Appl. Phys. **127**, 040901 (2020). https://doi.org/10.1063/1.5129365
4. Yao, G.Y.; Zhao, Z.Y.; Liu, Q.L.; Dong, X.D.; Zhao, Q.M.: Theoretical calculations for localized surface plasmon resonance effects of Cu/TiO2 nanosphere: Generation, modulation, and application in photocatalysis. Sol. Energy Mater. Sol. Cells **208**, 110385 (2020). https://doi.org/10.1016/j.solmat.2019.110385
5. Amendola, V.; Pilot, R.; Frasconi, M.; Marago, O.M.; Lati, M.A.: Surface plasmon resonance in gold nanoparticles: a review. J. Phys. Condens. Matter (2017). https://doi.org/10.1088/1361-648X/aa60f3
6. Asenjo-Garcia, A.; Manjavacas, A.; Myroshnychenko, V.; García de Abajo, F.J.: Magnetic polarization in the optical absorption of metallic nanoparticles. Opt. Express **20**(27), 28142–28152 (2012). https://doi.org/10.1364/OE.20.028142
7. Monticone, F.; Alu, A.: Metamaterial, plasmonic and nanophotonic devices. Rep. Progress Phys. (2017). https://doi.org/10.1088/1361-6633/aa518f
8. Jin, H.; Lin, G.; Bai, L.; Amjad, M.; Filho, E.P.B.; Wen, D.: Photothermal conversion efficiency of nanofluids: an experimental and numerical study. Sol. Energy **139**, 278–289 (2016). https://doi.org/10.1016/j.solener.2016.09.021
9. Yan, H.; Song, X.; Wang, X.; Wang, Y.: Electromagnetic wave absorption and scattering analysis for Fe_3O_4 with different scales particles. Chem. Phys. Lett. **723**, 51–56 (2019). https://doi.org/10.1016/j.cplett.2019.03.033
10. Vos, M.; Grande, P.L.: Simple model dielectric functions for insulators. J. Phys. Chem. Solids **104**, 192–197 (2017). https://doi.org/10.1016/j.jpcs.2016.12.015
11. Porfyrakis, P.; Tsitsas, N.L.: Nonlinear electromagnetic metamaterials: aspects on mathematical modeling and physical phenomena. Microelectron. Eng. **216**, 111028 (2019). https://doi.org/10.1016/j.mee.2019.111028

12. Fedorova, I.V.; Eliseeva, S.V.; Sementsov, D.I.: Spectral and polarization properties of a planar multiferroic structure. Opt. Commun. **458**, 124881 (2019). https://doi.org/10.1016/j.optcom.2019.124881
13. Xie, H.N.; Larmour, I.A.; Smith, W.E.; Faulds, K.; Graham, D.: Surface-enhanced Raman scattering investigation of hollow gold nanospheres. J. Phys. Chem. C **116**(14), 8338–8342 (2012). https://doi.org/10.1021/jp3014089
14. Farooq, S.; de Araujo, R.E.: Engineering a localized surface plasmon resonance platform for molecular biosensing. Open J. Appl. Sci. **8**(3), 126–139 (2018). https://doi.org/10.4236/ojapps.2018.83010
15. Ferdows, M.; Alzahrani, F.: Study of non-isothermal incompressible flow and heat flux of nano-ferrofluid with induced magnetic induction. Int. Commun. Heat Mass Transf. **109**, 104352 (2019). https://doi.org/10.1016/j.icheatmasstransfer.2019.104352
16. Chen, J.; Qi, S.; Hong, X.; Gu, P.; Wei, R.; Tang, C.; Huang, Y.; Zhao, C.: Highly sensitive 3D metamaterial sensor based on diffraction coupling of magnetic plasmon resonances. Results Phys. **15**, 102791 (2019). https://doi.org/10.1016/j.rinp.2019.102791
17. Halder, S.; Bhuyan, S.; Das, S.N.; Sahoo, S.; Choudhary, R.N.P.; Das, P.; Parida, K.: Structural, morphological, dielectric and impedance spectroscopy of lead-free Bi(Zn2/3Ta1/3)O3 electronic material. Appl. Phys. A Mater. Sci. Process. **123**, 781 (2017). https://doi.org/10.1007/s00339-017-1406-3
18. Deb, K.; Bera, A.; Bhowmik, K.L.; Saha, B.: Conductive polyaniline on paper as a flexible electronic material with controlled physical properties through vapor phase polymerization. Polym. Eng. Sci. **58**, 2249–2255 (2018). https://doi.org/10.1002/pen.24845
19. Pham, T.S.; Bui, H.N.; Lee, J.W.: Wave propagation control and switching for wireless power transfer using tunable 2-D magnetic metamaterials. J. Magn. Magn. Mater. **485**, 126–135 (2019). https://doi.org/10.1016/j.jmmm.2019.04.034
20. Hu, Z.; Kanagaraj, J.; Hong, H.; Yang, K.; Fan, Q.H.; Kharel, P.: Characterization of ferrite magnetic nanoparticle modified polymeric composites by modeling. J. Magn. Magn. Mater. **493**, 165735 (2020). https://doi.org/10.1016/j.jmmm.2019.165735
21. Xia, W.; Lu, J.; Tan, S.; Liu, J.; Zhang, Z.: Manipulating dielectric properties by modifying molecular structure of polymers. Dielectr. Polym. Mater. High Density Energy Storage (2018). https://doi.org/10.1016/B978-0-12-813215-9.00004-X
22. Devilez, A.; Zambrana-Puyalto, X.; Stout, B.; Bonod, N.: Mimicking localized surface plasmons with dielectric particles. Phys. Rev. B Condens. Matter Mater. Phys. **92**, 241412 (2015). https://doi.org/10.1103/PhysRevB.92.241412
23. Zhou, N.; Yan, R.; Wang, X.; Fu, J.; Zhang, J.; Li, Y.; Sun, X.: Tunable thickness of mesoporous ZnO-coated metal nanoparticles for enhanced visible-light driven photoelectrochemical water splitting. Chemosphere **273**, 129679 (2021). https://doi.org/10.1016/j.chemosphere.2021.129679
24. Avasthi, D.K.; Mishra, Y.K.; Singhal, R.; Kabiraj, D.; Mohapatra, S.; Mohanta, B.; Gohil, N.K.; Singh, N.: Synthesis of plasmonic nanocomposites for diverse applications. J. Nanosci. Nanotechnol. **10**(4), 2705–2712 (2010). https://doi.org/10.1166/jnn.2010.1433
25. Myroshnychenko, V.; Rodríguez-Fernández, J.; Pastoriza-Santos, I.; Funston, A.M.; Novo, C.; Mulvaney, P.; Liz-Marzán, L.M.; Abajo, F.J.G.D.: Modelling the optical response of gold nanoparticles. Chem. Soc. Rev. **37**(9), 1792–1805 (2008). https://doi.org/10.1039/b711486a
26. Tzarouchis, D.; Sihvola, A.: Light scattering by a dielectric sphere: perspectives on the Mie resonances. Appl. Sci. **8**(2), 184 (2018). https://doi.org/10.3390/app8020184
27. Bech, H.; Leder, A.: Two-particle characterization by pulse induced and time resolved Mie scattering. Optik **122**, 37–43 (2011). https://doi.org/10.1016/j.ijleo.2009.10.006
28. Aizpurua, J.; Hanarp, P.; Sutherland, D.S.; Kall, M.; Bryant, G.W.; Abajo, F.J.G.D.: Optical properties of gold nanorings. Phys. Rev. Lett. **90**, 057401 (2003). https://doi.org/10.1103/PhysRevLett.90.057401
29. Bi, K.; Zeng, L.; Chen, H.; Fang, C.; Wang, Q.; Lei, M.: Magnetic coupling effect of Mie resonance-based metamaterial with inclusion of split ring resonators. J. Alloys Compd. **646**, 680–684 (2015). https://doi.org/10.1016/j.jallcom.2015.05.247
30. Hu, W.; Yi, N.; Sun, S.; Cui, L.; Song, Q.; Xiao, S.: Enhancement of magnetic dipole emission at yellow light in optical metamaterials. Opt. Commun. **350**, 202–206 (2015). https://doi.org/10.1016/j.optcom.2015.03.077
31. Li, W.; Wei, J.; Wang, W.; Hu, D.; Li, Y.; Guan, J.: Ferrite-based metamaterial microwave absorber with absorption frequency magnetically tunable in a wide range. Mater. Des. **110**, 27–34 (2016). https://doi.org/10.1016/j.matdes.2016.07.118
32. Navarrete, J.; Siefe, C.; Alcantar, S.; Belt, M.; Stucky, G.D.; Moskovits, M.: Merely measuring the UV-visible spectrum of gold nanoparticles can change their charge state. Nano Lett. **18**(2), 669–674 (2018). https://doi.org/10.1021/acs.nanolett.7b02592
33. Fiedler, J.; Thiyam, P.; Kurumbail, A.; Burger, F.A.; Walter, M.; Persson, C.; Brevik, I.; Parsons, D.F.; Bostrom, M.; Buhmann, S.Y.: Effective polarizability models. J. Phys. Chem. A **121**(51), 9742–9751 (2017). https://doi.org/10.1021/acs.jpca.7b10159
34. Liu, W.; McLeod, E.: Accuracy of the skin depth correction for metallic nanoparticle polarizability. J. Phys. Chem. C **123**(20), 13009–13014 (2019). https://doi.org/10.1021/acs.jpcc.9b01672
35. Zhao, Q.; Zhou, J.; Zhang, F.; Lippens, D.: Mie resonance-based dielectric metamaterials. Mater. Today **12**(12), 60–69 (2009). https://doi.org/10.1016/S1369-7021(09)70318-9